Reaction of NO_2 with Zn and ZnO: Photoemission, XANES, and Density Functional Studies on the Formation of NO_3

José A. Rodriguez,*,† Tomas Jirsak,† Joseph Dvorak,† Sharadha Sambasivan,‡ and Daniel Fischer‡,§

Departments of Chemistry and National Synchrotron Light Source, Brookhaven National Laboratory, Upton, New York 11973, and Materials Science and Engineering Laboratory, National Institute of Standards and Technology Gaithersburg, Maryland 20899

Received: September 13, 1999; In Final Form: November 4, 1999

Synchrotron-based high-resolution photoemission and X-ray absorption near-edge spectroscopy (XANES) have been used to study the interaction of NO_2 with polycrystalline surfaces of metallic zinc and zinc oxide. NO_2 exhibits a complex chemistry on metallic zinc. After adsorbing nitrogen dioxide, N, O, NO, NO_2, and NO_3 are present on the surface of the metal. At room temperature the NO_2 molecule mainly dissociates into O adatoms and gaseous NO, whereas at low temperatures (<250 K) chemisorbed NO_2 and NO_3 dominate on the surface. NO_2 is a very good oxidizing agent for preparing ZnO from metallic zinc. Zn reacts more vigorously with NO_2 than metals, such as Rh, Pd, or Pt which are typical catalysts for the removal of NO_x molecules ($DeNO_x$ process). At 300 K, the main product of the reaction of NO_2 with polycrystalline ZnO is adsorbed NO_3 with little NO_2 or NO present on the surface of the oxide. No evidence was found for the full decomposition of the NO_2 molecule (i.e., no $NO_2 \rightarrow N + 2O$). The results of density functional (DF-GGA) calculations for the adsorption of NO_2 on a six-layer slab of ZnO, or INDO/S calculations for NO_2 on a $Zn_{37}O_{37}$ cluster, show stronger chemisorption bonds on (0001) Zn-terminated terraces than on $(000\bar{1})$ O-terminated terraces. The $Zn \leftrightarrow NO_2$ interactions on ZnO are strong and the Zn sites probably get oxidized and nitrated as a result of them. It appears that NO_2 is very efficient for fully oxidizing metal centers that are missing O neighbors in oxide surfaces. On zinc oxide, the nitrate species are stable up to temperatures near 700 K. ZnO can be useful as a sorbent in $DeNO_x$ operations.

I. Introduction

Nitrogen oxides (NO_2 and NO), one of the most harmful environmental poisons,[1] are formed in automotive engines and industrial combustion systems by thermal fixation and oxidation of atmospheric nitrogen.[2] The decomposition rate of the nitrogen oxides is low, and thus it is necessary to use catalysts or sorbents to remove them ($DeNO_x$ process).[2] Although the elimination of NO_x from gas streams has been a major concern for the last 3 decades, recently, research in this area has intensified.[2,3−6] In part, this is motivated by the fact that there is evidence that the emission of these noxious vapors into the atmosphere has increased.[3a,7] Also new and more stringent regulations on NO_x emissions have encouraged increasing interest in more efficient $DeNO_x$ operations.[2,5] The catalysts used in these operations frequently contain supported metals (Rh, Pd, Co, Cu, Au, etc.),[2,4−6] but metal oxides such as ZnO are able to catalyze the reduction of NO_2 by alkanes.[3b,8] Previous studies indicate that zinc oxide is a good sorbent for SO_2 ($DeSO_x$ process).[9] It is worthwhile to investigate if the same system can be useful for $DeSO_x$ and $DeNO_x$ operations. Here, we study the chemistry of NO_2 on metallic zinc and ZnO using synchrotron-based high-resolution photoemission, X-ray absorption near-edge spectroscopy (XANES) and density functional (DF) calculations.

Several studies have appeared in the literature examining the adsorption of NO_2 on transition metal surfaces.[10−18] At 300 K, NO_2 decomposes to adsorbed NO and O on Ru,[10] Rh,[11] Pd,[12] Pt,[13] and Ag.[14] Complete dissociation has been observed on W[15] and Mo,[16] while the least reactive metal is Au which leaves the chemisorbed NO_2 intact.[17] At higher temperatures (500−700 K), the decomposition of NO_2 produces a large amount of adsorbed oxygen and gaseous NO and/or N_2 on Ru,[10a] Mo,[16] Cu,[18] and Pd.[12] In this respect, NO_2 is a much better oxidizing agent than O_2:[10a,18,12] oxide multilayers are formed even after dosing NO_2 to flat surfaces such as Ru(001)[10a] or Mo(110).[16] At low temperatures, adsorbed NO_3 has been detected as the product of the reaction of NO_2 and adsorbed atomic oxygen on Ag(110).[14b] This nitrate species dissociates at temperatures above 450 K to yield gaseous NO_2 and NO plus oxygen adatoms. The NO_3 is attached to the Ag(110) substrate through only one of the oxygen atoms and has C_{2v} symmetry.[14b,c]

In principle the chemistry of NO_2 on oxide surfaces can be complex, since the molecule can interact with metal and/or oxygen centers. There is little literature available examining in detail the interaction of NO_2 with pure oxide surfaces.[19,20] On α-Fe_2O_3, NO_2 chemisorbs as such or as a dimer (N_2O_4) at low temperatures, but at ~400 K nitrate is the dominant species on the surface.[21] The formation of NO_3 was found after adsorbing NO_2 on heterogeneous catalysts that contain TiO_2,[22] V_2O_5,[22] Al_2O_3,[23] and ZrO_2,[23] or on hydroxylated TiO_2.[24] The results of temperature programmed desorption suggest the existence of adsorbed NO_3 after exposing CuO to NO_2 at 300 K.[3b]

* Corresponding author. FAX: (631) 344-5815. E-mail: rodrigez@bnl.gov.
† Department of Chemistry.
‡ National Synchrotron Light Source.
§ Materials Science and Engineering Laboratory.

10.1021/jp993224g CCC: $19.00
Published on Web 12/22/1999

Our results indicate that metallic zinc is extremely reactive toward NO_2 even at temperatures as low as 150 K. Clear evidence is found for the presence of several nitrogen species (N, NO, NO_2, NO_3) on metallic zinc. A rich chemistry is also observed for NO_2 on zinc oxide, and the molecule interacts with O and Zn centers of this substrate. NO_2 is very efficient for fully oxidizing metal centers that are missing O neighbors in ZnO. Stable NO_3 species are formed on the oxide at ~150 K and decompose at temperatures well above 500 K.

II. Experimental and Theoretical Methods

II.1. Work with Films of Zinc and Zinc Oxide. The photoemission experiments for the adsorption of NO_2 on polycrystalline films of metallic zinc and ZnO were performed in a conventional ultrahigh vacuum (UHV) chamber that is part of the U7A beamline of the National Synchrotron Light Source (NSLS) at Brookhaven National Laboratory. This UHV chamber contains a hemispherical electron energy analyzer with multichannel detection, instrumentation for low-energy electron diffraction (LEED), a quadrupole mass spectrometer, and a Mg Kα X-ray source. The N 1s and valence spectra were taken using a photon energy of 480 eV, whereas a photon energy of 625 eV was used to collect the O 1s data. The binding energy scale of the photoemission spectra was calibrated by the position of the Fermi edge in the valence band. Mg Kα radiation was used to take the Zn LMM Auger spectra.

Thick films of metallic zinc were vapor deposited on a clean Rh(111) substrate at 100 or 300 K. The evaporation of Zn was achieved by heating a W filament wrapped with ultrapure Zn wire. The formation of Zn multilayers was confirmed by the complete disappearance of the Rh photoemission features. ZnO films (>10 monolayers thick) were grown on the clean Rh(111) crystal using procedures described elsewhere.[25] In short, Zn atoms were vapor deposited under an O_2 atmosphere (1×10^{-6} Torr) on the Rh(111) substrate at 100 K. This was followed by heating of the sample (~1 K/s) to 700 K in the presence of 1×10^{-5} Torr of O_2. Following this methodology, one gets quasi-layer-by-layer growth and the ZnO films are polycrystalline (no LEED pattern was observed) with electronic properties and a phonon structure that are identical to those of bulk zinc oxide.[18,26] The Rh(111) crystal was mounted on a manipulator that allowed resistive heating to 1300 K and liquid-nitrogen cooling to 100 K. A type C thermocouple attached to the back of the Rh(111) substrate was used to measure the temperatures.

NO_2 was dosed to the polycrystalline Zn and ZnO surfaces through a glass capillary array doser positioned to face the sample at a distance of ~2 mm. The NO_2 exposures are based on the ion gauge reading and were not corrected for the capillary array enhancement.

II.2. Work with Zinc Oxide Powders. Bulk powders of zinc oxide (Aldrich, 99.9% purity) were exposed to 450−500 Torr (1 Torr= 133.32 N/m^2 or Pa) of NO_2 in a reaction cell[9b] for 10 min at 100 or 300 K. Before exposure to nitrogen dioxide, the ZnO powders were heated at 650 K under vacuum for 20 min to induce desorption of any OH groups that could be present on the surface. This was followed by "oxidation" of the sample under a 30%-O_2/70%-N_2 mixture (500 Torr, 15 min) at 500 K. Such a procedure led to powders that exhibited the typical O 1s XPS,[27,28] Zn LMM Auger,[28] and O K-edge XANES[29] spectra of ZnO. The N and O K-edge XANES data for the NO_2/ZnO systems were collected at the NSLS in beamline U7A. These spectra were taken in the "electron-yield mode" by using a channeltron multiplier located near the sample surface. The energy resolution was close to 0.3 eV.

II.3. Computational Methods. Calculations for the adsorption of NO_2 on periodic slabs of ZnO were performed within the density functional (DF) theory approach using a commercial version of CASTEP (Cambridge Serial Total Energy Package)[30] from Molecular Simulations, Inc. In this code, the wave functions of the valence electrons are expanded in a basis set of plane waves with kinetic energy smaller than a specified cutoff energy E_{cut}. The presence of tightly bound core electrons is represented by nonlocal ultrasoft pseudopotentials.[31] Reciprocal-space integration over the Brillouin Zone is approximated through a careful sampling at a finite number of *k*-points using the Monkhorst−Pack scheme.[32] The exchange-correlation contribution to the total electronic energy is treated in the generalized gradient corrected (GGA)[33] form of the local density approximation. In all the calculations, the kinetic energy cutoff E_{cut} and the density of Monkhorst-Pack k-point mesh were chosen high enough in order to ensure convergence of the computed structures and energetics. A large body of existing work indicates that CASTEP is excellent for predicting structural geometries and energy changes associated with chemical transformations.[30,34−36]

Due to the delocalized (plane wave) nature of its basis set, CASTEP is not particularly useful to investigate localized charges or electronic properties of individual atoms. To do this, we performed INDO/S calculations for NO_2 on ZnO clusters. INDO/S is a semiempirical method[37] that can give qualitative information about (1) the charge transfers associated with the chemisorption bond, (2) what atoms of the adsorbate and surface are involved in the chemisorption bond, (3) the changes in the strength of the bonds of the adsorbate that occur during the chemisorption process, and (4) the molecular-orbital energy-level spectrum of the adsorption complex.[38,39] In the past MO−SCF calculations based on this method have provided a reliable picture for the bonding mechanism of many molecules on zinc oxide[39] and NO_2 or NO_3 on silver.[14c] In this study, the parameters for N, O and Zn in the INDO/S calculations are those previously used in refs 14c and 39a.

III. Results

III.1. Reaction of NO_2 with Metallic Zinc. Figure 1 shows N and O 1s photoemission spectra acquired after dosing NO_2 to polycrystalline zinc at 280 K. In the O 1s region, there are two clear peaks at ~530.8 and 533.5 eV. The peak at lower binding energy indicates the existence of ZnO,[27,28] whereas the peak at higher binding energy is typical of NO_x species.[11a] The corresponding N 1s spectra show weak features at ~396.5 eV (N[11a,16,40]) and 401 eV (NO[11a,40]) and a strong peak at ~404.5 eV. This binding energy is between those reported for adsorbed NO (400−401.5 eV[11a,40]) and NO_3 (407−408 eV[41]), and we tentatively assign the peak to chemisorbed NO_2.[41] The validity of this assignment will be justified in section III.2. From these results we can conclude that around room temperature metallic zinc reacts vigorously with NO_2 and ZnO is mainly formed through the reaction

$$NO_2(gas) + Zn(solid) \rightarrow NO(gas) + ZnO(solid) \quad (1)$$

The chemisorbed NO_2 molecules in Figure 1 desorb or decompose during heating from 280 to 400 K, and at the end the system contains mostly ZnO and a small amount of N and NO.

Figures 2 and 3 display valence photoemission and Zn LMM Auger spectra taken before and after dosing NO_2 to zinc films

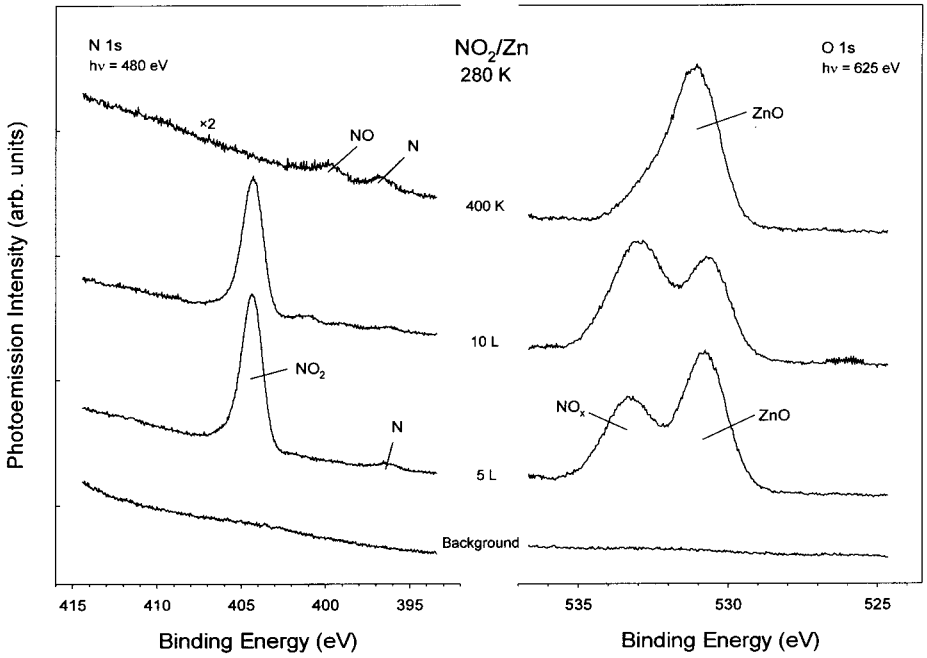

Figure 1. N and O 1s photoemission spectra for the adsorption of 5 and 10 L of NO_2 on metallic zinc at 280 K. In the final step, the sample was heated to 400 K. The electrons were excited using photon energies of 480 eV (N 1s) and 625 eV (O 1s).

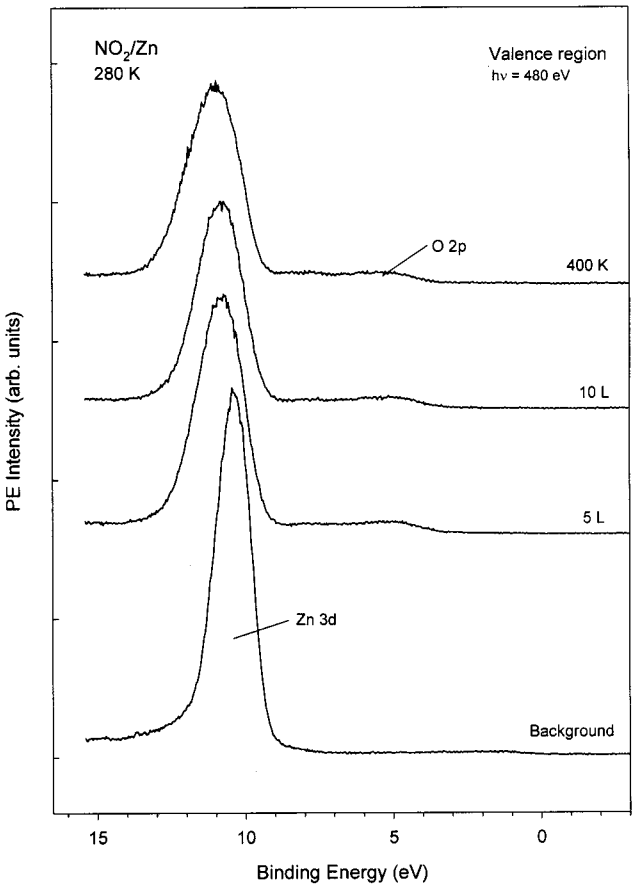

Figure 2. Valence spectra acquired in the same set of experiments that produced the N and O 1s spectra in Figure 1.

at 280−300 K. These data show quite clearly that Zn is being oxidized by reaction with NO_2. The valence spectra were taken with a photon energy of 480 eV, and therefore, the contributions from the O and N 2p levels are relatively weak. The dosing of NO_2 induces a positive binding-energy shift ($\sim$ 0.5 eV) in the Zn 3d levels and features for the O 2p levels appear between 7 and 3.5 eV. This is consistent with the formation of ZnO.[42] The Zn $L_3M_{45}M_{45}$ Auger transition is very sensitive to the formation of bonds between Zn and O.[43] A comparison of the Zn $L_3M_{45}M_{45}$ Auger peaks of bulk ZnO and metallic Zn shows large changes in the line shape and a difference of $\sim$4 eV in the peak positions.[43] In Figure 3, for an NO_2 exposure of four langmuirs (L), the corresponding Zn LMM spectrum shows that most of the Zn in the film is still not oxidized. A large amount of "Zn^{2+}" ions are present after an NO_2 dose of 20 L. Annealing from 300 to 800 K induces migration of oxygen into the bulk and desorption of metallic zinc.[44] At 800 K, the sample exhibits a Zn LMM Auger spectrum that is identical to that of polycrystalline ZnO.[28,43b] The oxidized Zn disappears upon annealing to 1100 K.

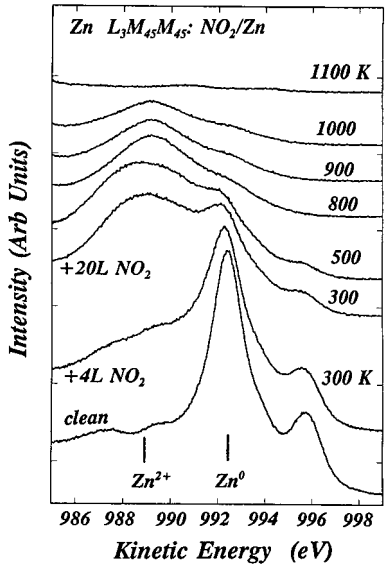

Figure 3. Zn LMM Auger spectra acquired after oxidizing a polycrystalline film of zinc with NO_2. First, 4 and 20 L of nitrogen dioxide were dosed at 300 K. Then, the sample was annealed to 500, 800, 900, 1000, and 1100 K. The Zn $L_3M_{45}M_{45}$ positions for the "Zn^{2+}" and "Zn^0" species were taken from ref 43. In these experiments, the primary electrons were excited with Mg Kα radiation.

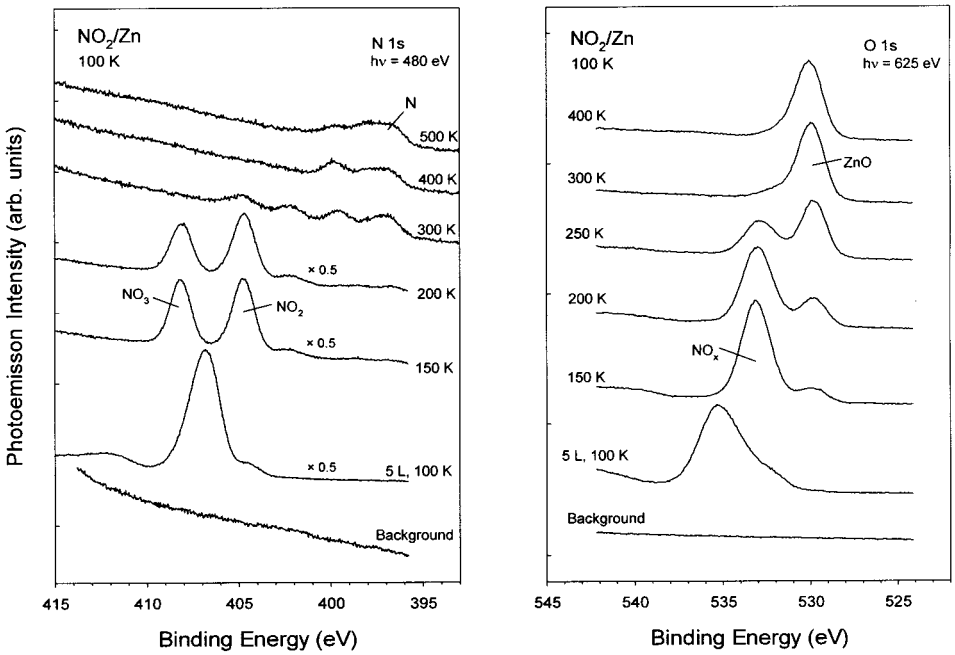

Figure 4. N and O 1s photoemission spectra for the adsorption of NO_2 on polycrystalline zinc at 100 K. After dosing, 5 L of the molecule the sample was heated to the indicated temperatures. The electrons were excited using photon energies of 480 eV (N 1s) and 625 eV (O 1s).

Figure 4 shows photoemission data for the adsorption of NO_2 on metallic zinc at ~ 100 K. An exposure of 5L of NO_2 leads to the deposition of a physisorbed multilayer of the N_2O_4 dimer[10b,11a] on the metal. Heating from 100 to 150 K induces the complete disappearance of this multilayer. At this point the O 1s spectrum shows a strong peak at ~ 533 eV that corresponds to NO_x species[11a] and a small peak at ~530 eV due to O bonded to Zn. In the N 1s region, there is no signal for atomic N (396−398 eV[11a,16,40]) and two intense peaks are seen at ~404 and 407.5 eV. These can be assigned to NO_2 and NO_3,[41] respectively. The NO_3 can be the product of the reactions

$$NO_2(gas) \rightarrow NO(gas) + O(ads) \quad (2)$$

$$NO_2(gas) + O(ads) \rightarrow NO_3(ads) \quad (3)$$

or a consequence of the disproportionantion of chemisorbed NO_2:

$$2NO_2(ads) \rightarrow NO(gas) + NO_3(ads) \quad (4)$$

In Figure 4, as the temperature is raised from 150 to 300 K, there is a substantial decrease in the signal for the NO_x species (probably due to desorption of NO and NO_2)[44b] and the peak for ZnO gains intensity. In the N 1s region at 300 K, weak features indicate the presence of small amounts of atomic N, NO, and NO_2. Final heating to 500 K leads to the disappearance of NO and NO_2 from the surface. At the end, the surface contains a small coverage of N and a lot of ZnO. The main difference between the results in Figures 1 (NO_2 dosing at 280 K) and 4 (NO_2 dosing at 100 K) is that at low temperatures NO_3 becomes a stable species on the surface. Both sets of results indicate that metallic zinc is extremely reactive toward NO_2.

III.2. Reaction of NO_2 with Zinc Oxide. The interaction between NO_2 and metallic Zn rapidly produces layers of ZnO. In this section we investigate the adsorption of NO_2 on polycrystalline films and bulk powders of ZnO. Figure 5 displays photoemission spectra for the adsorption of NO_2 on a thick film of zinc oxide. The N 1s spectrum at the bottom shows that the ZnO surface is essentially nitrogen free before beginning the dosing of NO_2. A trace of N at ~399 eV comes from the presence of residual NO_2 and NO gases in the UHV chamber during the preparation of the ZnO film.[25] This is not a problem since upon interaction with NO_2 the atomic N was oxidized to NO_x species. In Figure 5, the dosing of NO_2 at 100 K produces multilayers of the N_2O_4 dimer[10b,11a] on the oxide substrate. Heating to 150 K induces the desorption of the physisorbed N_2O_4 and facilitates the reaction

$$NO_2(ads) + ZnO(solid) \rightarrow ZnNO_3(solid) \quad (5)$$

At 200 K a peak for NO_3 at ~407 eV[41] dominates the N 1s region, with a small peak for NO_2 at ~404 eV.[41] NO_3 is clearly the main N species in the region near the surface (first 2−3 layers) probed by photoemission. The NO_2 features disappear upon annealing to 400 K. Further heating to 700 K leads to complete decomposition of the NO_3 producing pure ZnO.

In a set of experiments, bulk powders of ZnO were exposed to moderate pressures of NO_2 (450−500 Torr) at 100 and 300 K. Figure 6 displays XANES data at the N K-edge for one of these systems and two common standards (KNO_3, KNO_2) which show the electronic transitions within the NO_3 and NO_2 groups. In the spectrum for the pure nitrate, the intense resonance at ~407 eV corresponds to $1s \rightarrow 2a_2''(\pi)$ electronic transitions, whereas the broad features between 410 and 420 eV probably come from excitations into the $5a_1'$ and $5e'$ empty σ orbitals of NO_3.[14c] In the case of the NO_2- salt, the first strong peak at ~402 eV is due to $1s \rightarrow 2b_1(\pi)$ electronic transitions, with the envelope from 407 to 417 eV probably resulting from excitations into the $7a_1$ and $5b_2$ vacant σ orbitals of nitrogen dioxide.[14c] In Figure 6, the spectrum for a ZnO powder exposed to NO_2 at 300 K exhibits resonances that indicate the presence of a large amount of NO_3. This is in excellent agreement with the photoemission results in Figure 5, supporting the assignment proposed above for the N 1s peaks. After exposing bulk powders of ZnO to NO_2 at 100 K and warming to 300 K, in the N K-edge region we saw a strong resonance at ~ 407 eV (NO_3) *and* weak peaks between 400 and 402 eV that could be attributed to a small amount of chemisorbed NO_2 or NO. These weak features disappeared upon heating to 350−400 K.

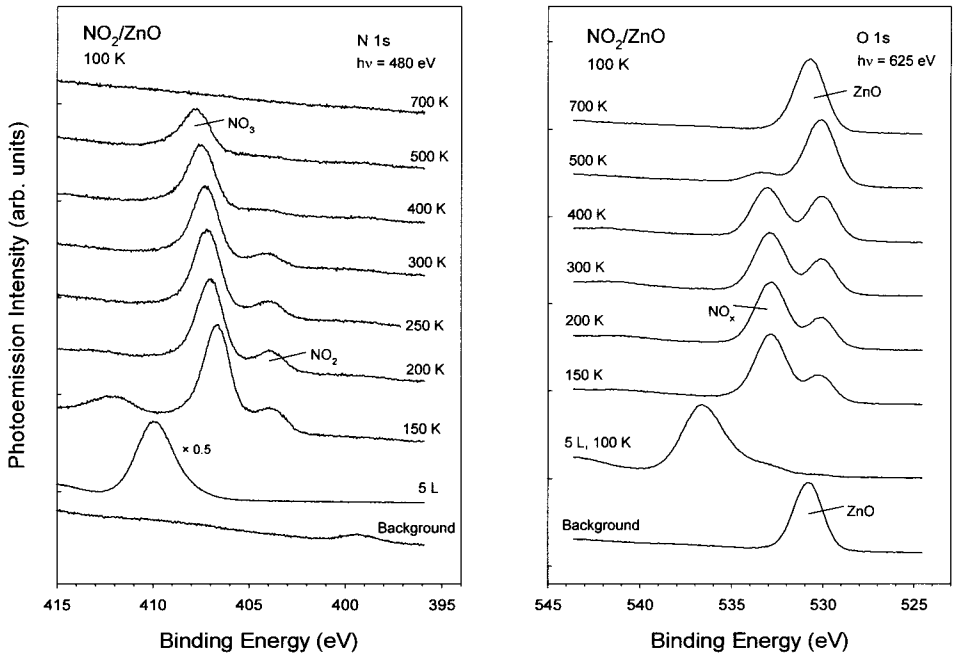

Figure 5. N and O 1s photoemission spectra for the adsorption of NO_2 on polycrystalline zinc oxide at 100 K. After dosing 5L of the molecule the sample was heated to the indicated temperatures. The electrons were excited using photon energies of 480 eV (N 1s) and 625 eV (O 1s).

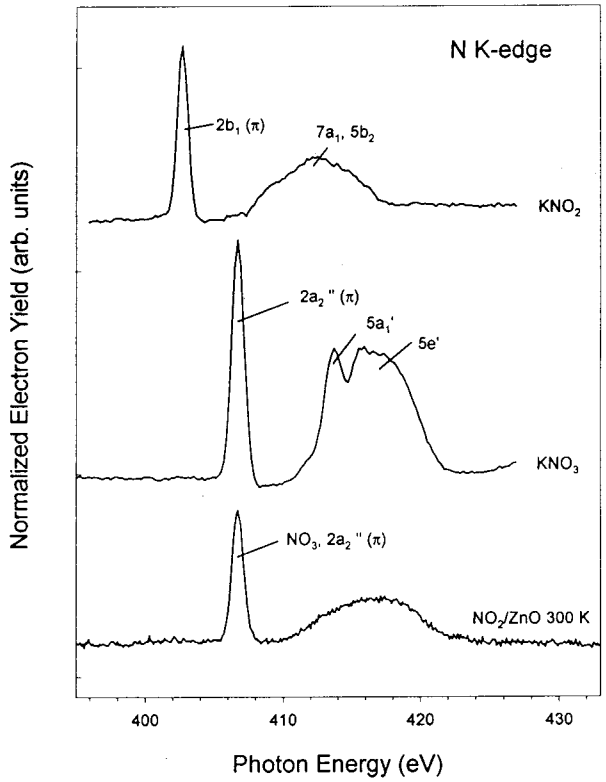

Figure 6. N K-edge XANES results for a ZnO powder exposed to NO_2 at 300 K. For comparison, we also include the results for two standards: KNO_2 and KNO_3.

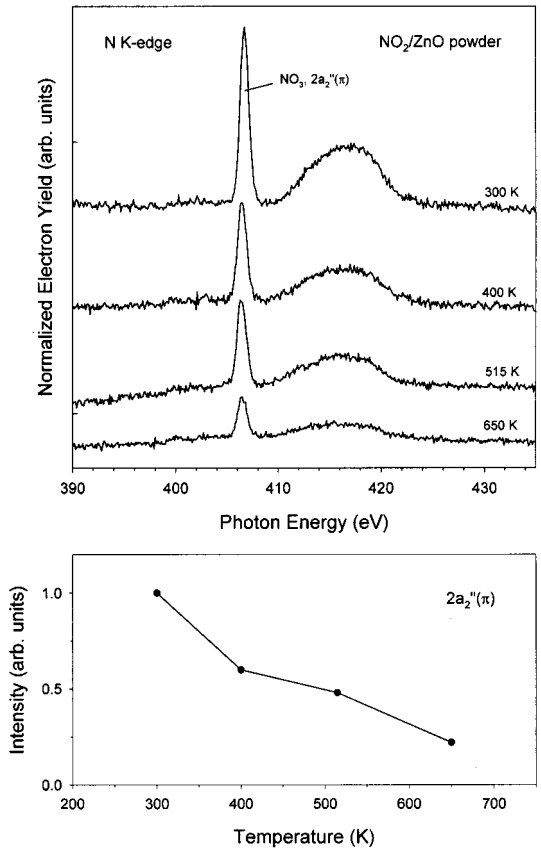

Figure 7. Top: N K-edge XANES spectra taken after exposing a bulk powder of ZnO to NO_2 (450 Torr) at 300 K and subsequent heating to 400, 515, and 650 K. Bottom: Intensity of the $2a_2''(\pi)$ resonance of NO_3 on ZnO as a function of annealing temperature.

Figures 7 and 8 display XANES results obtained after heating a NO_2/ZnO system to elevated temperatures. After dosing NO_2 to the oxide powder at 300 K, the N K-edge indicates that NO_3 is formed on the sample and this produces a significant change in the line-shape of the O K-edge (535−540 eV region). When the temperature is increased from 300 to 650 K, one sees a continuous decrease in the intensity of the NO_3 resonances in the N K-edge and the line-shape in the O K-edge gets more similar to that of pure ZnO. This agrees qualitatively with trends found in the photoemission experiments of Figure 5 which indicate that the nitrate is not stable at temperatures near 700 K.

The results in Figures 5 and 6 indicate that NO_3 is the dominant species in the NO_2/ZnO systems with only a small amount of NO_2 or NO bonded to Zn sites of the oxide. The

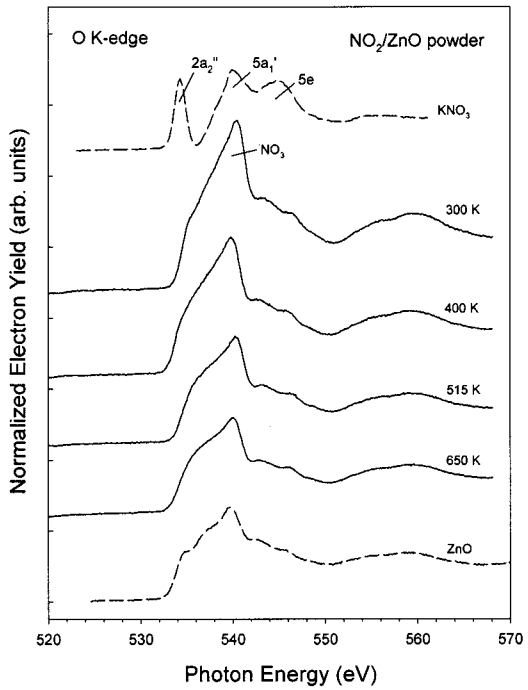

Figure 8. O K-edge XANES spectra taken after exposing a bulk powder of ZnO to NO_2 (450 Torr) at 300 K and subsequent annealing to 400, 515, and 650 K. For comparison, we also include results for pure (bottom) ZnO and (top) KNO_3.

surfaces under study here are polycrystalline and should contain a substantial amount of coordinatively unsaturated zinc atoms.[9,19] These Zn atoms could be unreactive toward NO_2, or they could be fully oxidized by a partial decomposition of the molecule with NO going into gas phase as seen on metallic zinc. In the next section, we will explore these two possibilities using density functional calculations.

III.3. Bonding Interactions of NO_2 with Zinc Oxide. Our main objective in this section is to compare the bonding interactions of NO_2 with Zn and O sites of zinc oxide. In particular, we are interested in the behavior of tri-coordinated Zn and O atoms (adsorption sites missing only one neighbor with respect to the tetracoordinated atoms in bulk ZnO[45]) which are very common on surfaces of zinc oxide.[19,42] For simplicity, we investigated the adorption of NO_2 on the Zn terminated, (0001)-Zn, and O terminated, $(000\bar{1})$-O, faces of ZnO.

Previous theoretical studies have shown that the use of infinite slabs is a valid and reliable approach for studying adsorption reactions on surfaces of zinc oxide.[46,47] In our density functional (DF) calculations the ZnO(0001) and ZnO$(000\bar{1})$ surfaces were modeled using an infinite slab that contained 3 layers of Zn and 3 layers of O arranged as shown in Figure 9. The top layer represents the (0001)-Zn face of ZnO, whereas the bottom layer is the $(000\bar{1})$-O face. The DF calculations were performed using three-dimensional periodic boundary conditions on a stack of slabs, each one being separated from its neighbors by a vacuum layer. The vacuum width was chosen equal to 12.5 Å to ensure that interactions between neighboring slabs were negligible.[34,46] The geometry optimization for bulk ZnO gave a wurtzite hexagonal unit cell with $a = b = 3.29$ Å and $c = 5.25$ Å. These values are very close to those derived from experimental measurements ($a = b = 3.25$ Å and $c = 5.21$ Å at 298 K[45]) and other theoretical calculations ($a = b = 3.29$ Å and $c = 5.24$ Å[46]). In the slab calculations, the structural geometries of the clean ZnO(0001) and ZnO$(000\bar{1})$ surfaces were determined by relaxing the two layers near each surface (one O layer, and one Zn layer) and keeping the other four layers of the slab in the geometry of bulk ZnO. In the case of ZnO(0001), the Zn outermost layer moved closer to the first oxygen layer by 0.23 Å (with respect to the separation seen for the (0001) plane of bulk ZnO). Such a relaxation has also been observed in LEED I−V experiments.[48] This relaxation was partially removed by adsorption of NO_2.

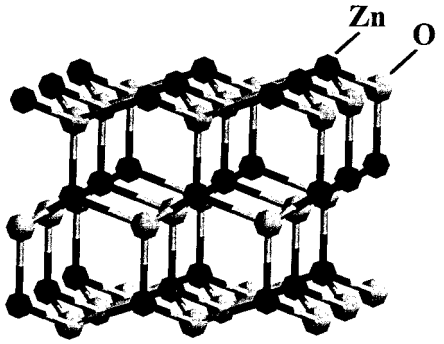

Figure 9. Section of the six-layer slab used to model the (0001)-Zn and $(000\bar{1})$-O faces of zinc oxide in the DF-GGA calculations. The Zn and O sites are denoted by dark and gray spheres, respectively. In the slab the first, third, and fifth layers contain only zinc atoms. The second, fourth, and sixth are oxygen layers. The first layer models the ZnO(0001)−Zn surface, whereas the sixth layer represents ZnO$(000\bar{1})$-O.

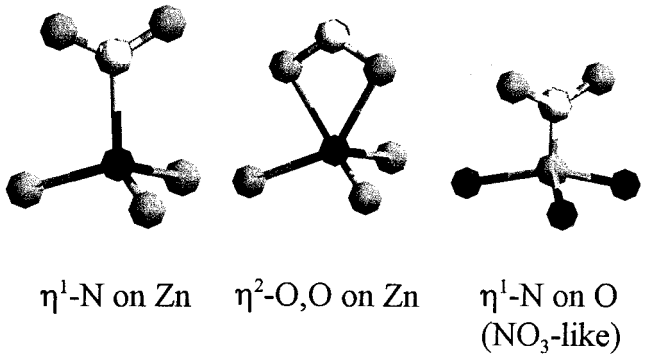

Figure 10. Bonding configurations of NO_2 on Zn (dark spheres) and O sites (grey spheres) of zinc oxide.

TABLE 1: Adsorption of NO_2 on ZnO(0001) and ZnO(0001): DF-GGA Results

	bond lengths (Å)				ads energy
	Zn_S-N	Zn_S-O	O_S-N	N−O	(kcal/mol)
free NO_2				1.21	
ZnO(0001)−Zn					
η^1-N (0.5 ML)	2.13	2.91		1.23	13
η^1-N (0.25 ML)	1.99	2.79		1.24	27
η^2-O,O (0.5ML)	2.58	2.16		1.27	21
η^2-O,O (0.25 ML)	2.55	2.12		1.28	38
ZnO$(000\bar{1})$−O					
η^1-N (0.5 ML)			1.49	1.22	12
η^1-N (0.25 ML)			1.43	1.22	26

The NO_2 molecule was adsorbed on the ZnO surfaces with the bonding configurations shown in Figure 10. The adsorption of NO_2 on the $(000\bar{1})$-O terminated surface produces an NO_3-like species. On the (0001)-Zn terminated face, NO_2 can bond via N (η^1-N) or the oxygens (η^2-O,O). Both bonding configurations have been observed on transition metal atoms.[14b,c,17] In the DF calculations the geometries of the adsorbate and the two substrate layers near the surface were optimized. Table 1 lists structural parameters and adsorption energies predicted by the DF calculations. Values are listed for NO_2 coverages of 0.5 and 0.25 ML. Following the usual convention,[34a] adsorption energies

TABLE 2: Adsorption of NO_2 on ZnO(0001) and ZnO(0001): INDO/S Results

	orbital populations (electrons)		charges (e)		bond order indices	
	σ	π	N	O	N−O	ZnO−NO_2
free NO_2	7.00	4.00	0.58	−0.29	1.60	
ZnO(0001)−Zn						
η^1-N	6.98	3.91	0.59	−0.24	1.51	0.64
η^2-O,O	7.30	3.89	0.35	−0.27	1.37	1.22
ZnO(000$\bar{1}$)−O						
η^1-N	6.90	3.84	0.92	−0.33	1.48	0.83

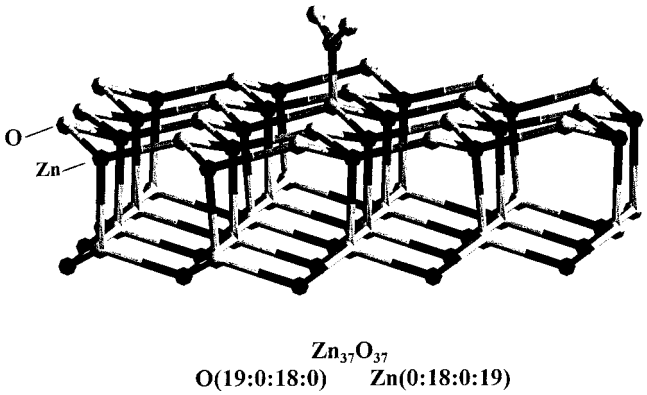

Figure 11. $Zn_{37}O_{37}$ cluster used in the INDO/S calculations. The Zn and O sites are denoted by dark and gray spheres, respectively. The cluster has four layers. The notation (a:b:c:d) specifies how many Zn or O atoms are in each layer. The first layer models the ZnO(0001)-O surface, whereas the fourth layer represents ZnO(0001)−Zn. The NO_2 molecule was adsorbed on the O atom shown in the figure, or on the Zn atom directly below in the fourth layer.

were calculated according to the expression

$$E_{ads} = E_{NO_2} + E_{slab} - E_{(NO_2+slab)} \quad (6)$$

where E_{NO_2} is the energy of the isolated NO_2 molecule in its equilibrium configuration, E_{slab} is the total energy of the bare slab, and $E_{(NO_2+slab)}$ is the total energy of the adsorbate/slab system. Positive adsorption energies denote an exothermic adsorption process. In Table 1, the bonding interactions of NO_2 with the Zn sites are much stronger than with the O sites. On a ZnO(0001)−Zn surface, bonding through the oxygens (η^2-O,O) is more stable than bonding via N (η^1-N). It is known that on Ag(110)[14b] and Au(111)[17] nitrogen dioxide adsorbs in a η^2-O,O configuration. In Table 1, the NO_2 adsorption energies decrease when the adsorbate coverage increases from 0.25 to 0.5 ML. Adsorbate↔adsorbate repulsive interactions substantially reduce the stability of NO_3 on ZnO(000$\bar{1}$)-O. This is consistent with the trends seen in the experimental results of Figures 5 and 7, where decomposition of NO_3 occurs in a large range of temperatures (∼300 K) with the molecule being much more stable at low coverages than at high coverages.

In the past MO−SCF calculations based on the INDO/S method[37] have provided a reliable picture for the bonding mechanism of many molecules on zinc oxide[39] and NO_2 on silver.[14c] Table 2 displays the results of INDO/S calculations for the adsorption of NO_2 on a $Zn_{37}O_{37}$ cluster (see Figure 11). Clusters of smaller size than this are frequently used to study adsorption reactions on zinc oxide.[9a,39,42a,49] A NO_2 molecule was bonded to the (000$\bar{1}$)-O or (0001)-Zn face of the $Zn_{37}O_{37}$ cluster with adsorption geometries derived from the DF calculations described above (θ_{NO2} = 0.25 ML in Table 1). The free NO_2 molecule is a radical ($^2A_1$ ground state[14c,50]) in which the HOMO, $6a_1$ orbital in Table 3, has σ symmetry and is only half occupied. The MO's immediately above and below the HOMO have π symmetry, $1a_2$ and $2b_1$ in Table 3. The INDO/S results indicate that the bonding mechanism of NO_2 on ZnO involves charge transfer from the $4b_2$ and $1a_2$ orbitals of the molecule into orbitals of the surface (σ- and π-donation) and charge transfer from the substrate into the half empty NO_2 $6a_1$ orbital (σ-back-donation). The transfer of electrons from ZnO toward the virtual $2b_1$, $7a_1$ and $5b_2$ orbitals of NO_2 is negligible. In Table 2, the calculated charge[52] on the N atom for a η^2-O,O coordination on ZnO(0001), the most stable conformation, is substantially lower (∼0.6e) than the N charge of a NO_3-like species on ZnO(000$\bar{1}$)-O. This type of difference leads to a big separation in the N peaks for NO_2 and NO_3 in photoemission (Figure 5) and XANES (Figure 6).

TABLE 3: NO_2 and NO_2^-: Energies of Molecular Orbitals (eV)

		NO_2^-	
	NO_2(INDO/S[a])	Ab initio SCF[b]	INDO/S
$5b_2$	20.7[c]		26.5[c]
$7a_1$	11.1[c]		17.4[c]
$2b_1(\pi)$	−0.9[c]		7.6[c]
$6a_1$	−11.3[d] (11.2)[e]	−3.9	−1.9
$1a_2(\pi)$	−12.5	−4.6	−4.6
$4b_2$	−12.4	−5.4	−5.1
$1b_1(\pi)$	−19.3	−10.6	−11.3
$5a_1$	−19.9	−11.7	−12.0
$3b_2$	−20.4	−11.1	−12.5

[a] Calculated using restricted open-shell Hartree−Fock (ROHF). [b] From ref 51. [c] Unoccupied orbital. [d] Half occupied orbital. [e] In parentheses is the experimental value for the first ionization potential of NO_2.[50] A detailed comparison of all the MO energies and experimental ionization potentials is presented in ref 14c.

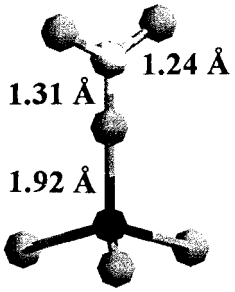

Figure 12. Structural parameters for the NO_3 formed on the ZnO(0001)−Zn surface upon reaction with NO_2 (θ_{NO3} = 0.25 ML).

The bond order indices[53] in Table 2 show a significant weakening in the N−O bonds of NO_2 upon adsorption of the molecule in a η^2-O,O coordination on ZnO(0001)−Zn. This facilitates the decomposition of NO_2 and subsequent oxidation of zinc. Using the slab in Figure 9 in combination with DF calculations, we found that the process

$$\equiv Zn + NO_2(gas) \rightarrow \equiv Zn-O + NO(gas) \quad (7)$$

$$\equiv Zn-O + NO_2(gas) \rightarrow \equiv Zn-ONO_2 \quad (8)$$

is exothermic on ZnO(0001). Stable NO_3 species are formed (see Figure 12), and the energy released depends on their final coverage: $\Delta E = -17$ kcal/mol at $\theta_{NO_3} = 0.25$ ML, and $\Delta E = -6$ kcal/mol at $\theta_{NO_3} = 0.5$ ML. Thus, the lack of intense NO_2 features in the experimental results of Figures 5 and 6 does not imply that the Zn sites of polycrystalline ZnO surfaces interact weakly with NO_2. The theoretical results in this section show that the Zn↔NO_2 interactions are strong and many Zn sites probably get oxidized or nitrated upon exposure to NO_2. This

is consistent with the trends seen in section III.1 in experiments for the reaction of NO_2 with metallic zinc.

IV. Discussion

IV.1. Interaction of NO_2 with Metallic Zinc. NO_2 exhibits a rich chemistry on pure zinc. After exposure to NO_2, photoemission shows the presence of N, O, NO, NO_2, and NO_3 on the surface of the metal. At room temperature the NO_2 molecule mainly dissociates into O adatoms and gaseous NO, whereas at low temperatures (<250 K) chemisorbed NO_2 and NO_3 dominate on the surface. Previous studies report that at 300 K nitrogen dioxide decomposes to adsorbed NO and O on Ru,[10] Rh,[11] Pd,[12] Pt,[13] Cu[18], and Ag.[14] Complete dissociation ($NO_2 \rightarrow N + 2O$) has been observed on W[15] and Mo.[16] Au leaves the chemisorbed NO_2 intact. Zinc is a Group 12 s,p metal that in comparison with transition and noble metals frequently displays a relatively low chemical affinity for many molecules.[44,54] This is not the case when interacting with NO_2. In fact, zinc reacts more vigorously with NO_2 than metals, such as Rh, Pd, or Pt, which are typical $DeNO_x$ catalysts.[5]

The chemistry of NO_2 on zinc at low temperatures (<250 K) is particularly interesting since large coverages of NO_3 are formed on the surface. This is different from the behavior seen on transition metals,[10−13,15,16] where the formation of nitrate species seems to be difficult. At low temperatures, adsorbed NO_3 has been detected as the product of the reaction of NO_2 and adsorbed atomic oxygen on Ag.[14b]

At high temperatures (500−700 K), the decomposition of NO_2 produces a large amount of adsorbed oxygen and gaseous NO and/or N_2 on Ru,[10a] Mo,[16] Cu[18], and Pd.[12] NO_2 is very efficient for synthesizing multilayers of RuO_x on Ru(001)[10a] or MoO_2 on Mo(110).[16] For preparing ZnO on surfaces of metallic Zn, NO_2 is a much better oxidizing agent than molecular oxygen. This correlates with the difference in the strength of the N−O ($NO_{2,gas} \rightarrow NO_{gas} + O_{gas}$, $\Delta H = 73$ kcal/mol)[55] and O−O bonds ($O_{2.gas} \rightarrow 2O_{gas}$, $\Delta H = 119$ kcal/mol).[55] O_2 exposures in excess of 5000 L are necessary in order to produce substantial amounts of ZnO on metallic Zn.[44b] This oxidation reaction is not practical for work under ultrahigh vacuum conditions. In contrast, repeating the experiments with NO_2 shown in Figure 3, one can obtain multilayers of pure oxidized zinc (i.e., no N) after heating to 700 K which have the electronic properties and phonon structure of bulk ZnO.[18]

IV.2. Interaction of NO_2 with Zinc Oxide. The photoemission and XANES results indicate that the main product of the reaction of NO_2 with polycrystalline ZnO is adsorbed NO_3. This species is stable on the oxide surface up to temperatures near 700 K. On α-Fe_2O_3, NO_2 exhibits a chemistry similar to that observed here for ZnO: the molecule chemisorbs as a dimer (N_2O_4) at very low temperatures and above room-temperature NO_3 is the dominant species on the surface.[21] The formation of NO_3 has been detected after adsorbing NO_2 on complex catalysts that contain TiO_2, V_2O_5, Al_2O_3, or ZrO_2.[22−24] Recent XANES studies for the reaction of NO_2 with a series of pure oxide powders (CeO_2, CuO, MgO, BaO) show a large amount of NO_3 and little NO_2 or NO on these systems at 300 K.[56]

The results of DF calculations indicate that the Zn↔NO_2 interactions on ZnO are strong and the Zn sites probably get oxidized or nitrated as a result of them. After adsorbing NO_2 on ZnO_{1-x} or Zn/ZnO surfaces, one sees a large decrease in the Zn $L_3M_{45}M_{45}$ signal for metallic zinc. Since a N−O bond in nitrogen dioxide is relatively easy to break ($NO_{2,gas} \rightarrow NO_{gas} + O_{gas}$, $\Delta H = 73$ kcal/mol),[55] it can be expected that in general the molecule will be very efficient for fully oxidizing metal centers that are missing O neighbors in oxide surfaces (i.e., elimination of O vacancies). This oxidation process will be followed by reaction of NO_2 with O centers and subsequent formation of NO_3. At the end, nitrate will be the main product of the interaction between NO_2 and the oxide.

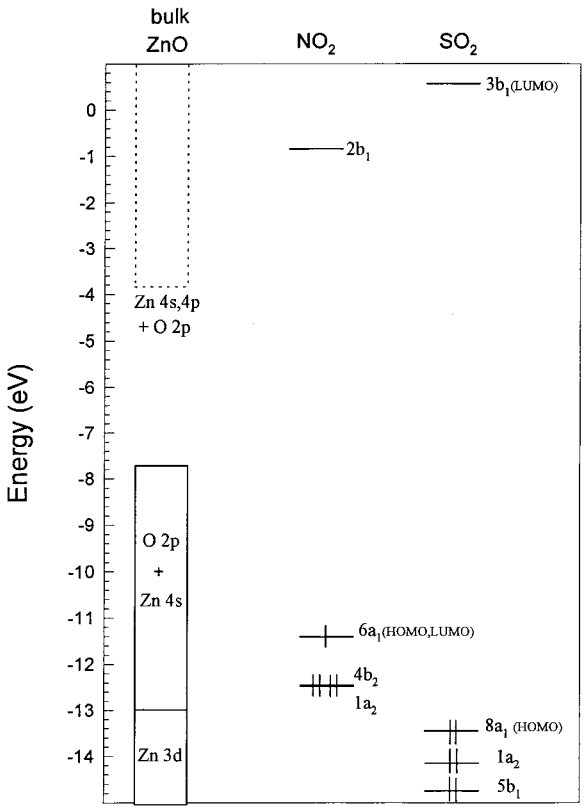

Figure 13. Energy range covered by the bands of ZnO[19,60] plus the MO's of NO_2 and SO_2.[60] The empty and occupied states of ZnO are indicated by dotted and solid lines, respectively. All the energies are reported with respect to the vacuum level.

NO_2 is a radical molecule and its bonding interactions with the metal centers of ZnO are much stronger than those seen for "simple" molecules such as CO,[19,39b,46b,49d] NH_3,[19,39c,49d] H_2O,[19,20,39c] and H_2.[19,20] Previous studies indicate that radical species (HCOO,[20,39c] CH_3O,[20,39c] CH_3S,[25a,49c] OH[19,20,39e], SH,[49c,57] HCC,[20,39a] Cl[39a]) interact very strongly with the cations of ZnO. CO_2[19,20] and SO_2[9] are able to react with the O centers of ZnO as does NO_2. CO_3 and SO_3 are stable species on zinc oxide.[9b,19,20]

Since zinc oxide is a good sorbent for SO_2 in $DeSO_x$ processes,[9] it is worthwhile to compare in detail the behavior of NO_2 and SO_2 on this oxide. The bonding interactions of SO_2 with the metal cations of ZnO, or other oxides such as MgO[58] and MoO_2,[59] are relatively weak and do not compete favorably with O↔SO_2 interactions.[9a] Figure 13 displays the molecular orbital energies of NO_2 and SO_2[60] plus the band energies of ZnO.[19,60] The interactions between the LUMO of SO_2 ($3b_1$ orbital) and the occupied orbitals of a metal play a predominant role in the energetics of the metal−SO_2 bond.[58,61] In Figure 13, the LUMO of SO_2 appears at much higher energy than the occupied Zn 4s band in ZnO, making Zn(4s)−$SO_2(3b_1)$ bonding interactions very difficult. On the other hand, in the case of NO_2, the $6a_1$ orbital is only half occupied and its energy position is ideal for electron donor−electron acceptor interactions with the occupied and empty states of Zn centers. These differences lead to strong Zn↔NO_2 and weak Zn↔SO_2 bonding interactions. The SO_3 and NO_3 species formed by reaction of the

adsorbates with O centers of zinc oxide display a similar thermal stability and survive on the oxide surface up to temperatures close to 700 K (Figure 7 and ref. [9b]). Our results indicate that ZnO can be useful as a sorbent in both $DeNO_x$ and $DeSO_x$ operations.

V. Conclusions

NO_2 exhibits a complex chemistry on metallic zinc. After adsorbing nitrogen dioxide, N, O, NO, NO_2, and NO_3 are present on the surface of the metal. At room temperature the NO_2 molecule mainly dissociates into O adatoms and gaseous NO, whereas at low temperatures ($<$250 K) chemisorbed NO_2 and NO_3 dominate on the surface. NO_2 is a very good oxidizing agent for preparing ZnO from metallic zinc. Zn reacts more vigorously with NO_2 than metals such as Rh, Pd, or Pt which are typical $DeNO_x$ catalysts.

At 300 K, the main product of the reaction of NO_2 with polycrystalline ZnO is adsorbed NO_3 with little NO_2 or NO present on the surface of the oxide. No evidence was found for the full decomposition of the NO_2 molecule (i.e., no $NO_2 \rightarrow N + 2O$). The $Zn \leftrightarrow NO_2$ interactions on ZnO are strong and the Zn sites probably get oxidized and nitrated as a result of them. It appears that NO_2 is very efficient for fully oxidizing metal centers that are missing O neighbors in oxide surfaces. On zinc oxide, the nitrate species are stable up to temperatures near 700 K. ZnO can be useful as a sorbent in $DeNO_x$ operations.

Acknowledgment. The authors thank A. Maiti from Molecular Simulations for his help with the use of the CASTEP program. The research carried out at Brookhaven National Laboratory was supported by the Division of Chemical Sciences of the U.S. Department of Energy (Contract DE-AC02-98CH10086). The NSLS is supported by the Divisions of Materials and Chemical Sciences of the U.S. Department of Energy. Certain commercial names are identified in this paper for the purpose of clarity in the presentation. Such identification does not imply endorsement by the National Institute of Standards and Technology.

References and Notes

(1) Stern, A. C.; Boubel, R. W.; Turner, D. B.; Fox, D. L. *Fundamentals of Air Pollution*, 2nd ed; Academic Press: Orlando, 1984.

(2) Lox, E. S. J.; Engler, B. H. In *Handbook of Heterogeneous Catalysis*; Ertl, G.; Knözinger, H., Weitkamp, J., Eds.; Wiley-VCH: Germany, 1997; pp 1559−1668.

(3) (a) Bélanger, R.; Moffat, J. B. *Applied Catal. B* **1997**, *13*, 167 (b) Shimokawabe, M.; Itoh, K.; Takezawa, N. *Catal. Today*, **1997**, *36*, 65.

(4) (a) Permana, H.; Ng, K. Y. S.; Peden, C. H. F.; Schmieg, S. J. Lambert, D. K.; Belton, D. N. **1996**, *164*, 194 b. Kim, Y. J.; Thevuthasan, S.; Herman, G. S.; Peden, C. H. F.; Chamberss, S. A.; Belton, D. M.; Permana, H. *Surf. Sci.* **1996**, *359*, 269.

(5) (a) Taylor, K. C. *Catal. Rev. Sci. Eng.* **1993**, *35*, 457. (b) Shelef, M.; Graham, G. W. *Catal. Rev. Sci. Eng.* **1994**, *36*, 433.

(6) (a) Cordatos, H.; Gorte, R. J. *Applied Catal. B* **1995**, *7*, 33 (b) Cordatos, H.; Gorte, R. J. *J. Catal.* **1996**, *159*, 112.

(7) (a) Lefohn, A. S.; Shadwick, D. S. *Atmos. Environ.* **1991**, *25A*, 491. (b) Tsai, S.; Bedell, S. A.; Kirby, L.; Zabcik, D. J. *Environ. Prog.* **1989**, *8*, 126.

(8) Shimokawabe, M.; Ohi, A.; Takezawa, N. *React. Kinet. Catal. Lett.* **1994**, *52*, 393.

(9) (a) Chaturvedi, S.; Rodriguez, J. A.; Jirsak, T.; Hrbek, J. *J. Phys. Chem. B* **1998**, *102*, 7033. (b) Rodriguez, J. A.; Jirsak, T.; Chaturvedi, S.; Kuhn, M. *Surf. Sci.* **1999**, *442*, 400.

(10) (a) Hrbek, J.; van Campen, D. G.; Malik, I. J. *J. Vac. Sci. Technol. A* **1995**, *13*, 1409. (b) Schwalke, U.; Parmeter, J. E.; Weinberg, W. H. *J. Phys. Chem.* **1986**, *84*, 4036.

(11) (a) Jirsak, T.; Dvorak, J.; Rodriguez, J. A. *Surf. Sci.* **1999**, *436*, L683. (b) Peterlinz, K. A.; Sibener, S. J. *J. Phys. Chem.* **1995**, *99*, 2817.

(12) Banse, B. A.; Koel, B. E. *Surf. Sci.* **1990**, *232*, 275.

(13) Bartram, M. E.; Windham, R. G.; Koel, B. E. *Surf. Sci.* **1987**, *184*, 57.

(14) (a) Polzonetti, G.; Alnot, P.; Brundle, C. R. *Surf. Sci.* **1990**, *238*, 226. (b) Outka, D. A.; Madix, R. J.; Fischer, G. B.; DiMaggio, C. *Surf. Sci.* **1987**, *179*, 1. (c) Rodriguez, J. A. *Surf. Sci.* **1990**, *230*, 335.

(15) Fuggle, J. C.; Menzel, D. *Surf. Sci.* **1979**, *79*, 1.

(16) Jirsak, T.; Kuhn, M.; Rodriguez, J. A. *Surf. Sci.* **2000**. In press.

(17) Bartram, M. E.; Koel, B. E. *Surf. Sci.* **1989**, *213*, 137.

(18) Rodriguez, J. A.; Hrbek, J. *J. Vac. Sci. Technol. A* **1994**, *12*, 2140.

(19) Henrich, V. E.; Cox, P. A. *The Surface Science of Metal Oxides*; Cambridge University Press: Cambridge, 1994; pp 273−275.

(20) Barteau, M. A. *Chem. Rev.* **1996**, *96*, 1413.

(21) Busca, G.; Lorenzelli, V. *J. Catal.* **1981**, *72*, 303.

(22) Dines, T. J.; Rochester, C. H.; Ward, A. W. *J. Chem. Soc., Faraday Trans.* **1991**, *87*, 643.

(23) Pozdnyakov, D. V.; Filimonov, V. N. *Kinet. Katal.* **1973**, *14*, 655.

(24) Kantcheva, M. M.; Bushev, V. P.; Hadjilvanov, K. I. *J. Chem. Soc., Faraday Trans.* **1992**, *88*, 3087.

(25) (a) Dvorak, J.; Jirsak, T.; Rodriguez, J. A. In preparation. (b) Jirsak, T.; Dvorak, J.; Rodriguez, J. A. *J. Phys. Chem. B* **1999**, *103*, 5550.

(26) Chaturvedi, S.; Rodriguez, J. A.; Hrbek, J. *Surf. Sci.* **1997**, *384*, 260.

(27) Campbell, C. T.; Daube, K. A.; White, J. M. *Surf. Sci.* **1987**, *182*, 458.

(28) Schön, G. *J. Electron Spectroscopy and Related Phenomena* **1973**, *2*, 75.

(29) Chen, J. G.; Frühberger, B.; Colaianni, M. L. *J. Vac. Sci. Technol. A* **1996**, *14*, 1668.

(30) Payne, M. C.; Allan, D. C.; Arias, T. A.; Johannopoulus, J. D. *Rev. Mod. Phys.* **1992**, *64*, 1045.

(31) Vanderbilt, D. *Phys. Rev. B* **1990**, *41*, 7892.

(32) Monkhorst, H. J.; Pack, J. D. *Phys. Rev. B* **1990**, 13, 5188.

(33) (a) Perdew, J. P.; Wang, Y.; *Phys. Rev. B*, **1992**, *46*, 6671. (b) White, J. A.; Bird, D. M. *Phys. Rev. B* **1994**, *50*, 4954.

(34) (a) Sorescu, D. C.; Yates, J. T. *J. Phys. Chem. B*, **1998**, *102*, 4556. (b) Robertson, I. J.; Thomson, D.; Heine, V.; Payne, M. C. *J. Phys.* **1994**, *6*, 9963. (c) White, J. A.; Bird, D. M.; Payne, M. C.; Stich, I. *Phys. Rev. Lett.* **1994**, *73*, 1404.

(35) Rodriguez, J. A.; Hanson, J. C.; Chaturvedi, S.; Maiti, A.; Brito, J. L. *J. Chem. Phys.* **2000**, *112*. In press.

(36) (a) Molteni, C.; Marzari, M. C.; Payne, M. C.; Heine, V. *Phys. Rev. Lett.* **1997**, *79*, 869. (b) Parlinski, K.; Li, Z. Q.; Kawazoe, Y. *Phys. Rev. Lett.* **1997**, *78*, 4063.

(37) (a) Anderson, W. P.; Edwards, W. D.; Zerner, M. C. *Inorg. Chem.* **1986**, *25*, 2728. (b) Zerner, M. C.; Loew, G. H.; Kirchner, R. F.; Mueller-Westerhoff, U. T. *J. Am. Chem.* Soc. **1980**, *102*, 589. (c) Bacon, A. D.; Zerner, M. C.; *Theor. Chim. Acta* **1979**, *53*, *21*.

(38) (a) Rodriguez, J. A.; Campbell, C. T. *Surf. Sci.* **1988**, *206*, 426. (b) Lindner, T.; Somers, J.; Bradshaw, A. M.; Williams, G. P. *Surf. Sci.* **1987**, *185*, 75. (c) Rodriguez, J. A.; Campbell, C. T. *Surf. Sci.* **1988**, *194*, 475. (d) Jirsak, T.; Rodriguez, J. A.; Chaturvedi, S.; Hrbek, J. *Surf. Sci.* **1998**, *418*, 8.

(39) (a) Rodriguez, J. A. *Surf. Sci.* **1989**, *222*, 383. (b) Rodriguez, J. A.; Campbell, C. T. *J. Phys. Chem.* **1987**, *91*, 6648. (c) Rodriguez, J. A.; Campbell, C. T. *Surf. Sci.* **1988**, *194*, 475. (d) Rodriguez, J. A.; Campbell, C. T. *Surf. Sci.* **1988**, *197*, 567. (e) Rodriguez, J. A. *Langmuir*, **1988**, *4*, 1006. (f) Rodriguez, J. A.; Chaturvedi, S.; Kuhn, M. *Surf. Sci.* **1998**, *415*, L1065.

(40) De Louise, L. A.; Winograd, N. *Surf. Sci.* **1985**, *159*, 199.

(41) Wagner, C. D.; Riggs, W. M.; Davis, L. E.; Moulder, J. F.; Muilenberg, G. E. *Handbook of X-ray Photoelectron Spectroscopy*; Perkin-Elmer: Eden-Praire, Minnesota, 1978; p 40.

(42) (a) Chaturvedi, S.; Rodriguez, J. A.; Hrbek, J. *J. Phys. Chem. B*, **1997**, *101*, 10860. (b) See p 143 in ref 19.

(43) (a) Wagner, C. D.; Gale, L. H.; Raymond, R. H. *Anal. Chem.* **1979**, *51*, 466. (b) Leighton, C. A.; Swift, A. J.; Vickerman, J. C. *Surf. Sci.* **1991**, *253*, 220.

(44) (a) Rodriguez, J. A.; Kuhn, M. *J. Phys. Chem.* **1996**, *100*, 381. (b) Rodriguez, J. A. *J. Phys. Chem.* **1993**, *97*, 6509.

(45) Abrahams, S. C.; Bernstein, J. L. *Acta Crystallogr. B* **1969**, *25*, 1233.

(46) (a) Jaffe, J. E.; Harrison, N. M.; Hess, A. C. *Phys. Rev. B* **1994**, *49*, 11153. (b) Jaffe, J. E.; Hess, A. C. *J. Chem. Phys.* **1996**, *104*, 3348.

(47) Baetzold, R. C. *J. Phys. Chem.* **1985**, *89*, 4150.

(48) Duke, C. B.; Lubinsky, A. R. *Surf. Sci.* **1975**, *50*, 605.

(49) (a) Anderson, A. B.; Nichols, J. A. *J. Am. Chem. Soc.* **1986**, *108*, 4742. (b) Sekine, R.; Adachi, H.; Morimoto, T. *Surf. Sci.* **1989**, *208*, 177. (c) Casarin, M.; Maccato, C.; Tondello, E.; Vittadini, *Surf. Sci.* **1995**, *343*, 115. (d) Casarin, M.; Tondello, E.; Vittadini, A. *Surf. Sci.* **1994**, *303*, 125.

(50) (a) Edqvist, O.; Lindholm, E.; Selin, L. E.; Åsbrink, L.; Kuyatt, C. E.; Mielczarek, S. R.; Simpson, J. A.; Fischer-Hjamars, I. *Phys. Scr.* **1970**, *1*, 172. (b) Brundle, C. R.; Neumann, D.; Price, W. C.; Evans, D.; Potts, A. W.; Streets, D. G. *J. Chem. Phys.* **1970**, *53*, 705.

(51) Considine, M.; Connor, J. A.; Hillier, I. H. *Inorg. Chem.* **1977**, *16*, 1392.

(52) (a) The reported charges were calculated by a Mulliken population analysis,[52b] using the overlap matrix and the deorthogonalized INDO eigenvector matrix.[52c] Due to the limitations of the Mulliken population analysis,[52d] the charges must be considered only in qualitative terms. (b) Mulliken, R. S. *J. Chem. Phys.* **1955**, *23*, 1841. (c) Shillady, D. D.; Billingsley, F. P.; Bloor, J. E. *Theor. Chim. Acta* **1971**, *21*, 1. (d) Szabo, A.; Ostlund, N. S. *Modern Quantum Chemistry*; McGraw-Hill: New York, 1982.

(53) (a) Wiberg, K. A. *Tetrahedron* **1968**, *24*, 1083. (b) Mayer, I. *Int. J. Quantum Chem.* **1986**, *29*, 73.

(54) Somorjai, G. A. *Introduction to Surface Chemistry and Catalysis*; Wiley: New York, 1994.

(55) Dean, J. A. *Lange's Handbook of Chemistry*, 13th ed.; McGraw-Hill: New York, 1985; pp 9−68, 3−131.

(56) Rodriguez, J. A.; Sambasivan, S.; Fischer, D. In preparation.

(57) Rodriguez, J. A.; Jirsak, T.; Chaturvedi, S.; Hrbek, J. *Surf. Sci.* **1988**, *407*, 171.

(58) Pacchioni, G.; Clotet, A.; Ricart, J. M. *Surf. Sci.* **1994**, *315*, 337.

(59) Jirsak, T.; Rodriguez, J. A.; Hrbek, J. *Surf. Sci.* **1999**, *426*, 319.

(60) Rodriguez, J. A.; Jirsak, T.; Hrbek, J. *J. Phys. Chem. B*, **1999**, *103*, 1966.

(61) Sakaki, S.; Sato, H.; Imai, Y.; Morokuma, K.; Ohkubo, K. *Inorg. Chem.* **1985**, *24*, 4538.